

The Persistence of High-Frequency Spin Fluctuations in Overdoped $\text{La}_{2-x}\text{Sr}_x\text{CuO}_4$ ($x=0.22$)

O.J. Lipscombe,¹ S.M. Hayden,¹ B. Vignolle,¹ D.F. McMorrow,² and T.G. Perring³

¹*H.H. Wills Physics Laboratory, University of Bristol, Tyndall Ave., Bristol, BS8 1TL, UK*

²*London Centre for Nanotechnology and Department of Physics and Astronomy, University College London, London, WC1E 6BT, UK*

³*ISIS Facility, Rutherford Appleton Laboratory, Chilton, Didcot, Oxfordshire OX11 0QX, United Kingdom*

We report a detailed inelastic neutron scattering study of the collective magnetic excitations of overdoped superconducting $\text{La}_{1.78}\text{Sr}_{0.22}\text{CuO}_4$ for the energy range 0–160 meV. Our measurements show that overdoping suppresses the strong response present for optimally doped $\text{La}_{2-x}\text{Sr}_x\text{CuO}_4$ which is peaked near 50 meV. The remaining response is peaked at incommensurate wavevectors for all energies investigated. We observe a strong high-frequency magnetic response for $E \gtrsim 80$ meV suggesting that significant antiferromagnetic exchange couplings persist well into the overdoped part of the cuprate phase diagram.

PACS numbers: 74.72.Dn, 74.25.Ha, 75.40.Gb, 78.70.Nx

The occurrence of high-temperature superconductivity is widely believed to be connected to the cuprates' spin degrees of freedom [1]. Thus, we might expect strong spin fluctuations to co-exist with superconductivity over the whole superconducting phase diagram. The spin excitations have been well characterised for the insulating antiferromagnetic (AF) [2] and lightly-doped [3, 4, 5, 6] compositions. For optimally doped compositions, structured excitations have been observed over a wide energy range [7, 8]. However, little is known about the high-energy spin dynamics on the overdoped side of the cuprate phase diagram. One of the best materials to investigate this region is single layer $\text{La}_{2-x}\text{Sr}_x\text{CuO}_4$ (LSCO). This system can be doped sufficiently to destroy the superconductive behavior [9], allowing the spin excitations to be studied across the entire superconducting dome. Studying the overdoped part of the phase diagram offers a different view on the emergence of the superconducting state. In contrast to the underdoped regime, superconductivity does not emerge from the 'pseudogap' state [10]. Rather, it emerges from what appears to be a strongly correlated metallic state [11].

In this letter, we report an inelastic neutron scattering (INS) study of the magnetic response $\chi''(\mathbf{q}, \omega)$ of an overdoped superconducting sample over a wide energy range (0–160 meV) and throughout the Brillouin zone. We have chosen the composition $\text{La}_{1.78}\text{Sr}_{0.22}\text{CuO}_4$ ($T_c = 26$ K), which shows a substantial drop in T_c with respect to optimal doping but is nevertheless superconducting (see Fig. 1). We find that the spin excitations are dramatically modified from those observed at optimal doping: The strong peak in the local susceptibility $\chi''(\omega)$ present [8] in $\text{La}_{1.84}\text{Sr}_{0.16}\text{CuO}_4$ near 50 meV is suppressed, and the remaining response is incommensurate and strongest around $E \approx 10$ meV and $E \gtrsim 80$ meV. Thus, strong spin excitations persist well into the overdoped region of the cuprate phase diagram as required by magnetically

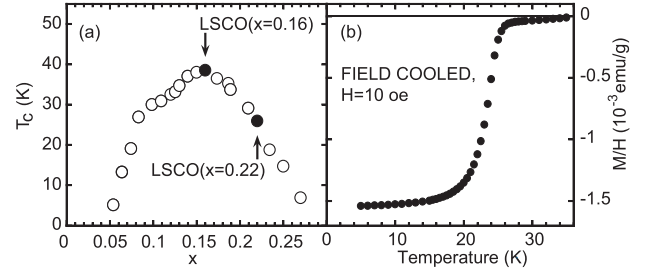


FIG. 1: (a) The doping dependence of T_c in $\text{La}_{2-x}\text{Sr}_x\text{CuO}_4$. Open circles [12], closed circles: LSCO($x=0.16$) [8] and LSCO($x=0.22$) (this work). (b) Magnetization of LSCO($x=0.22$) used in this work ($H=10$ oe $\parallel c$, field cooled).

mediated models of superconductivity.

$\text{La}_{1.78}\text{Sr}_{0.22}\text{CuO}_4$ has a tetragonal structure and we use tetragonal indexing to label reciprocal space $\mathbf{Q} = h\mathbf{a}^* + k\mathbf{b}^* + l\mathbf{c}^*$. The magnetic excitations in LSCO are 2D as the strongest magnetic couplings are within the CuO_2 planes. Thus, usually we quote in-plane components of \mathbf{Q} . In this notation, the parent compound of the series, La_2CuO_4 , exhibits AF order with an ordering vector of $(1/2, 1/2)$ and \mathbf{a}^* points along the Cu–O bonds. Seven single crystals with a total mass of 75 g were co-aligned with a total mosaic of 0.8° . The crystals were grown by a traveling-solvent floating-zone technique [13] and annealed with one bar of oxygen for six weeks at 800°C . The Sr stoichiometry was measured with SEM-EDX and ICP-AES to be $x = 0.215 \pm 0.005$. Magnetization measurements [see Fig. 1(b)] indicate that $T_c(\text{onset}) = 26$ K.

INS probes the energy and wavevector dependence of $\chi''(\mathbf{q}, \omega)$. The magnetic cross section is given by

$$\frac{d^2\sigma}{d\Omega dE} = \frac{2(\gamma r_e)^2 k_f}{\pi g^2 \mu_B^2 k_i} |F(\mathbf{Q})|^2 \frac{\chi''(\mathbf{q}, \hbar\omega)}{1 - \exp(-\hbar\omega/kT)}, \quad (1)$$

where $(\gamma r_e)^2 = 0.2905$ barn sr^{-1} , \mathbf{k}_i and \mathbf{k}_f are the inci-

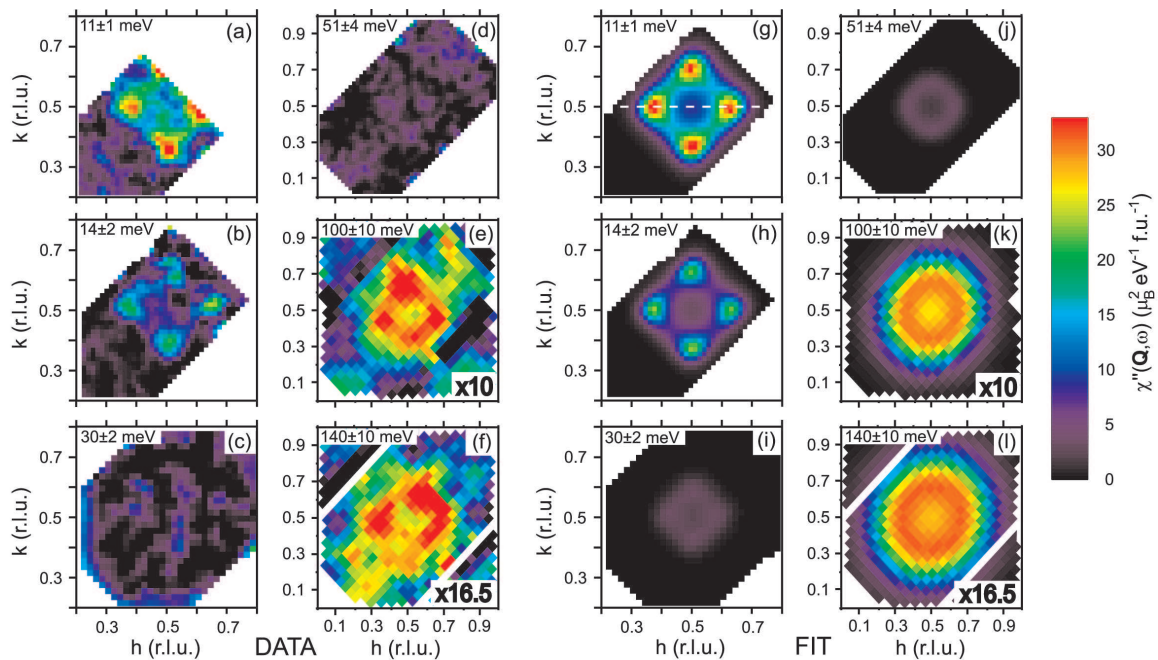


FIG. 2: (color online) (a)–(f) Constant- E slices of $\chi''(\mathbf{q}, \omega)$ for $\text{La}_{1.78}\text{Sr}_{0.22}\text{CuO}_4$ at $T = 6$ K. Data are cut off due to finite detector coverage. (g)–(l) Fits of model (Eq. 2) convolved with instrument resolution. (a) and (b) show the low- E four-peak structure which is suppressed in (c) and (d). (e) and (f) show the reemergence of a ring-like response at high energy. (a)–(d) have same intensity ranges, (e) and (f) are $\times 10$ and $\times 16.5$ respectively. E_i 's for (a)–(f) were 40, 40, 90, 120, 160, 240 meV.

dent and final neutron wavevectors and $|F(\mathbf{Q})|^2$ is the anisotropic magnetic form factor for a Cu^{2+} $d_{x^2-y^2}$ orbital. Data were placed on an absolute scale using a V standard.

The magnetic response of the cuprates is dominated by the unpaired $3d$ electrons of Cu^{2+} ions. The AF parent compound La_2CuO_4 displays spin waves [2], which disperse out from $(1/2, 1/2)$ position. For doped superconducting compositions, the low-energy ($E \lesssim 20$ meV) excitations of $\text{La}_{2-x}\text{Sr}_x\text{CuO}_4$ are peaked at $(1/2 \pm \delta, 1/2)$ and $(1/2, 1/2 \pm \delta)$ [14, 15]. The low-energy incommensurability of the excitations δ increases with x and saturates with $\delta \approx 0.125$ [9, 12]. It has recently been shown that $\delta(E)$ of $\text{La}_{2-x}\text{Sr}_x\text{CuO}_4$ and $\text{La}_{2-x}\text{Ba}_x\text{CuO}_4$ disperses [8, 16, 17] with energy and shows a minimum near $E \approx 50$ meV. The high-energy ($E > 50$ meV) response in optimally doped $\text{La}_{1.84}\text{Sr}_{0.16}\text{CuO}_4$ appears to be more isotropic, possibly with incommensurate (IC) peaks rotated by $\pi/4$ in the (h, k) plane [8]. Interestingly, a similar ‘hourglass’ dispersion has been observed [6, 18, 19] in $\text{YBa}_2\text{Cu}_3\text{O}_{6+x}$.

Our INS experiments were performed on the MAPS instrument at the ISIS spallation source. MAPS is a direct-geometry time-of-flight chopper spectrometer with position-sensitive detectors. This allows a large region of reciprocal space to be sampled using a single setting with a given incident energy E_i . In order to identify and minimize phonon contamination of our results we collected data for seven different E_i 's. Each E_i al-

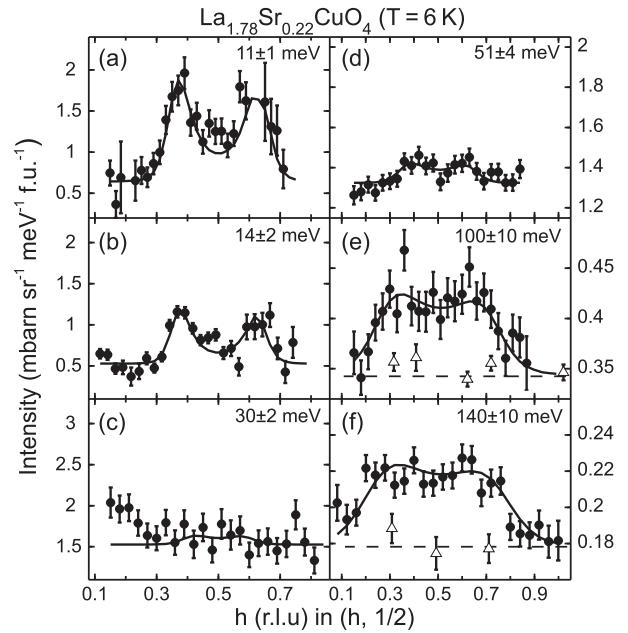


FIG. 3: (a)–(f) Constant- E cuts through the raw data [see trajectory in Fig. 2(g)]. A background proportional to $|\mathbf{Q}|^2$ has been subtracted. The energies are the same as the slices in Fig. 2. Solid lines are fits of Eq. 2 convolved with the instrument resolution. Background points (Δ) for (e)–(f) measured along $(h, 0.05)$. Scattering near $h=0.2$ in (c) is due to phonons.

lows a given (h, k, E) position to be probed for a different l value [see Fig 4(d)]. The magnetic scattering in LSCO depends only on the out-of-plane wavevector l through $|F(\mathbf{Q})|^2$, whereas phonon scattering is strongly dependent on l . We excluded data from our final results if it satisfied any of the following criteria: (i) A clearly identified phonon branch could be seen to cross the $(1/2, 1/2)$ region. (ii) The pattern was not four-fold symmetric around $(1/2, 1/2)$ (after subtracting a background quadratic in \mathbf{Q}). (iii) The fitted value of $\chi''(\omega)$ was more than twice (including errors) that found at the same E for a different E_i . The excluding procedure was only required below the phonon cut-off energy of 90 meV.

Fig. 2 shows $\chi''(\mathbf{q}, \omega)$ of LSCO($x=0.22$) as slices at various energies. Corresponding cuts through the raw data along the $(h, 1/2)$ line are plotted in Fig. 3. The low- E cut in Fig. 2(a) at $E=11$ meV shows the well-known four-peak structure [8, 9, 12, 14, 15, 16, 17]. The structure is considerably weaker at $E=14$ meV [Fig. 2(b) and Fig. 3(b)] and has almost disappeared for $E=30$ meV and $E=50$ meV [Fig. 2(c)-(d) and Fig. 3(c)-(d)]. This behavior is in contrast to optimally doped $\text{La}_{1.84}\text{Sr}_{0.16}\text{CuO}_4$ [8, 17], where the IC response is strongest around $E \approx 20$ meV and there is a strong response centered on $(1/2, 1/2)$ for energies in the range $E=40$ –50 meV. At higher energies, the magnetic response reemerges for $E=100$ meV [Fig. 2(e) and Fig. 3(e)] and $E=140$ meV [Fig. 2(f) and Fig. 3(f)]. The high- E response is significantly broader in \mathbf{q} and $\chi''(\mathbf{q}, \omega)$ is weaker than the low- E response. However, as we shall see below, when integrated in \mathbf{q} and E it dominates the magnetic response.

We used a modified lorentzian function to make a quantitative analysis of the data:

$$\chi''(\mathbf{q}, \omega) = \chi_\delta(\omega) \frac{\kappa^4(\omega)}{[\kappa^2(\omega) + R(\mathbf{q})]^2} \quad (2)$$

with

$$R(\mathbf{q}) = \frac{[(h - \frac{1}{2})^2 + (k - \frac{1}{2})^2 - \delta^2]^2 + \lambda(h - \frac{1}{2})^2(k - \frac{1}{2})^2}{4\delta^2},$$

where the position of the four peaks is determined by δ , κ is an inverse correlation length (peak width), and λ controls the shape of the pattern ($\lambda=4$ yields four distinct peaks and $\lambda=0$ a pattern with circular symmetry [20]). This phenomenological response function provides a good description of the data at all energies. Fig. 2(g)-(l) show 2D fits of Eq. 2 to the corresponding slices (a)-(f). The parameters extracted from fitting the resolution-convolved model to the 2D slices are shown in Fig. 4(a)-(c). We have expressed the strength of the magnetic response in terms of the wavevector-averaged or local susceptibility $\chi''(\omega) = \int \chi''(\mathbf{q}, \omega) d^3q / \int d^3q$ determined from the fitted $\chi''(\mathbf{q}, \omega)$. The local susceptibility indicates the overall strength of the magnetic excitations for a given energy.

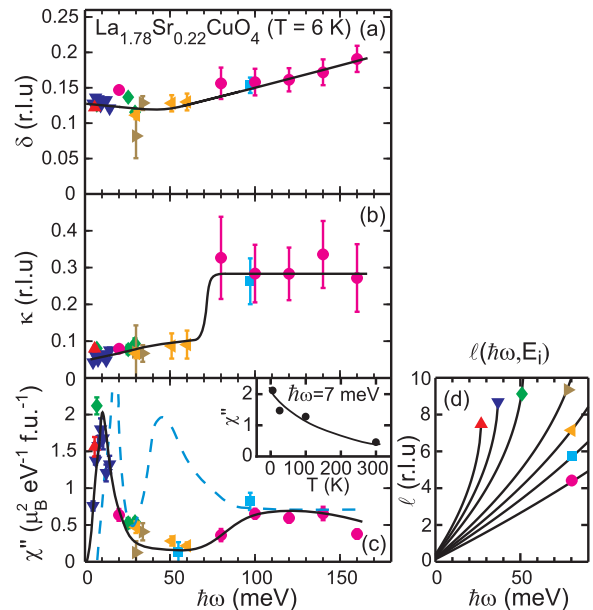


FIG. 4: (color online). (a)–(c) E -dependence of δ , κ and $\chi''(\omega)$ in LSCO($x=0.22$). δ , κ define the dispersion, and $\chi''(\omega)$ the strength of the spin excitations. The inset shows how the response at 7 meV weakens on warming. Dashed line in (c) is $\chi''(\omega)$ in LSCO($x=0.16$) for comparison [8]. Lines are guides to the eye. (d) E -dependence of out-of-plane wavevector, l , at $(1/2, 1/2)$ for each E_i . Symbols indicate E_i : 30 (\blacktriangle), 40 (\blacktriangledown), 55 (\blacklozenge), 90 (\blacktriangleright), 120 (\blacktriangleleft), 160 (\blacksquare), 240 meV (\bullet).

Fig. 4 summarizes the main findings of this work. Firstly, the magnetic response is made up of two components [see Fig. 4(c)]: A low-frequency (four-peaked) component for which $\chi''(\omega)$ is peaked around $E \approx 10$ meV and a much broader high-frequency component which is strongest around $E \approx 120$ meV. The spectral weight of the components are found to be 0.028(3) and 0.053(4) $\mu_B^2 \text{f.u.}^{-1}$, the high energy component therefore dominating the response. The emergence of the high-frequency component at $E \approx 80$ meV corresponds to a rapid broadening of $\chi''(\mathbf{q}, \omega)$ in wavevector as shown by the sudden increase in the κ parameter [Fig. 4(b)] at this energy. Comparing the present results with a recent study [8] of optimally doped $\text{La}_{1.84}\text{Sr}_{0.16}\text{CuO}_4$ over the same energy range [dashed line is Fig. 4(c)], we note (i) The low-energy peak in $\chi''(\omega)$ has moved from 18 meV down to about 10 meV with no change in spectral weight [21]. The low-energy IC component [Fig. 4(a)] does not disperse rapidly towards $(1/2, 1/2)$ as seen in optimally doped LSCO [8, 17]. Instead the pattern disappears rapidly. (ii) The peak in $\chi''(\omega)$ around 40-60 meV present in LSCO($x=0.16$), which corresponds to a strong response near $(1/2, 1/2)$, is suppressed. (iii) A high-energy ($E \gtrsim 80$ meV) component remains with approximately the same amplitude as for LSCO($x=0.16$). A recent study [22] of more highly doped LSCO($x=0.25$) reported significant spectral weight in the range 40-60

meV, although we note that this work was performed with two E_i 's only, which may have limited the ability to discriminate between scattering of a magnetic and phononic nature.

The origin of the magnetic excitations in the cuprates has been discussed in terms of many models. As we move to the overdoped side of the phase diagram, it is widely believed that Fermi-liquid-based models become more appropriate. Within such models, the low-energy IC peaks arise from the creation of (correlated) quasiparticle pairs [23, 24, 25]. Thus the shift of the low-energy peak in $\chi''(\omega)$ to lower energy as we move from LSCO($x=0.16$) to overdoped LSCO($x=0.22$) might be due to changes in the band structure. It is more difficult to explain the sudden collapse of the magnetic response in the intermediate 50–70 meV energy range between LSCO($x=0.16$) and LSCO($x=0.22$) [see Fig. 4(c)] although photoemission (ARPES) suggests that the topology of the Fermi surface changes between these two compositions as the quasiparticle states near $(1/2, 0)$ move above the Fermi energy [26]. Thus, there will undoubtedly be a concomitant change in the nesting of the quasiparticle states. At higher energies (80–160 meV), we observe the reemergence of a magnetic signal which despite the heavy doping is about 1/3 of the intensity of the parent antiferromagnet La_2CuO_4 [7] in the same energy range. If we associate the high-energy response with residual antiferromagnetic interactions, we find from the dispersion of the high-energy excitations [Fig. 4(a)] $dE/d|\delta| = 1800 \pm 500$ meV r.l.u. $^{-1}$ that $J = 180 \pm 50$ meV. Thus a strong AF exchange coupling persists across the cuprate phase diagram into the overdoped region.

It is interesting to compare our measurements with electronic spectroscopies. ARPES experiments [27, 28, 29] have observed ‘kink’ structures in the quasiparticle dispersion of a number of systems including LSCO. These have been interpreted as a signature of the coupling of quasiparticles to collective excitations (bosons). In LSCO($x=0.22$) a kink is observed [29] at about 70 meV which corresponds approximately to the onset of the higher-energy excitations that we have observed. Recent APRES experiments [30, 31, 32, 33] indicate further quasiparticle anomalies at higher energies which persist into the overdoped region [30]. These features could be related to high-energy spin fluctuations which have been observed up to 250 meV for LSCO($x=0.14$) [7] and up to 160 meV in the present measurement of LSCO($x=0.22$). Infrared optical-spectroscopy measurements [34] also provide evidence of the coupling of quasiparticles to bosonic excitations and in particular the existence of a two-component excitation spectrum with a high-energy tail.

In conclusion, overdoping dramatically suppresses the magnetic response. The remaining spin excitations are incommensurate and persist over a wide energy range. Defining the energy scale of the spin excitations as the

‘center of mass’ of the observed spectrum, the parent compound is an antiferromagnet with spin-wave excitations and an energy scale $E \approx 2J \approx 300$ meV. Doping results in stronger magnetic excitations at intermediate energies, $E \approx 50$ meV, for example, in optimally doped $\text{La}_{2-x}\text{Sr}_x\text{CuO}_4$ and a lower energy scale. The present experiment shows that the energy scale increases as we move into the overdoped regime. Thus, the special feature of the optimally doped region is the overall low characteristic energy of the spin excitations and the drop in T_c with overdoping is associated with the disappearance of the commensurate response near 50 meV [8].

-
- [1] A. V. Chubukov, D. Pines, and J. Schmalian, in *The Physics of Superconductors*, Eds. K. H. Bennemann and J. B. Ketterson (Springer, Berlin, 2003), vol. 2, p. 495.
 - [2] R. Coldea, *et al.*, Phys. Rev. Lett. **86**, 5377 (2001).
 - [3] B. Keimer, *et al.*, Phys. Rev. B **46**, 14034 (1992).
 - [4] C. Stock, *et al.*, Phys. Rev. B **73**, 100504 (2006).
 - [5] H. A. Mook, *et al.*, Phys. Rev. Lett. **88**, 097004 (2002).
 - [6] S. M. Hayden, H. A. Mook, P. C. Dai, T. G. Perring, and F. Dogan, Nature **429**, 531 (2004).
 - [7] S. M. Hayden, *et al.*, Phys. Rev. Lett. **76**, 1344 (1996).
 - [8] B. Vignolle, *et al.*, Nature Phys. **3**, 163 (2007).
 - [9] S. Wakimoto, *et al.*, Phys. Rev. Lett. **92**, 217004 (2004).
 - [10] T. Timusk and B. Statt, Rep. Prog. Phys. **62**, 61 (1999).
 - [11] N. Hussey, M. Abdel-Jawad, A. Carrington, A. Mackenzie, and L. Balicas, Nature **425**, 814 (2003).
 - [12] K. Yamada, *et al.*, Phys. Rev. B **57**, 6165 (1998).
 - [13] S. Komiyama, Y. Ando, X. F. Sun, and A. N. Lavrov, Phys. Rev. B **65**, 214535 (2002).
 - [14] G. Shirane, *et al.*, Phys. Rev. Lett. **63**, 330 (1989).
 - [15] S. W. Cheong, *et al.*, Phys. Rev. Lett. **67**, 1791 (1991).
 - [16] J. M. Tranquada, *et al.*, Nature **429**, 534 (2004).
 - [17] N. B. Christensen, *et al.*, Phys. Rev. Lett. **93**, 147002 (2004).
 - [18] M. Arai, *et al.*, Phys. Rev. Lett. **83**, 608 (1999).
 - [19] P. Bourges, *et al.*, Science **288**, 1234 (2000).
 - [20] The data is best described with $\lambda = 4(1 - E/E_\lambda)$ for $E < E_\lambda$ and $\lambda = 0$ for $E \geq E_\lambda$, where $E_\lambda = 60$ meV.
 - [21] For LSCO($x=0.16$) [8], the total spectral weight of the low and high energy components are 0.031(3) and 0.110(8) μ_B^2 f.u. $^{-1}$.
 - [22] S. Wakimoto, *et al.*, Phys. Rev. Lett. **98**, 247003 (2007).
 - [23] Q. M. Si, Y. Y. Zha, K. Levin, and J. P. Lu, Phys. Rev. B **47**, 9055 (1993).
 - [24] P. B. Littlewood, J. Zaanen, G. Aeppli, and H. Monien, Phys. Rev. B **48**, 487 (1993).
 - [25] M. R. Norman, cond-mat/0701720.
 - [26] T. Yoshida, *et al.*, Phys. Rev. B **74**, 224510 (2006).
 - [27] A. Kaminski, *et al.*, Phys. Rev. Lett. **86**, 1070 (2001).
 - [28] P. D. Johnson, *et al.*, Phys. Rev. Lett. **87**, 177007 (2001).
 - [29] X. J. Zhou, *et al.*, Nature **423**, 398 (2003).
 - [30] A. A. Kordyuk, *et al.*, Phys. Rev. Lett. **97**, 17002 (2006).
 - [31] J. Graf, *et al.*, Phys. Rev. Lett. **98**, 067004 (2007).
 - [32] T. Valla, *et al.*, Phys. Rev. Lett. **98**, 167003 (2007).
 - [33] J. Chang, *et al.*, cond-mat/0610880.
 - [34] J. Hwang, *et al.*, cond-mat/0610488.